AGU ADVANCING EARTH AND SPACE SCIENCE

Geophysical Research Letters

RESEARCH LETTER
10.1029/2021GL093596

The Longest 2020 Meiyu Season Over the Past 60 Years: Subseasonal Perspective and Its Predictions

Shaobo Qiao[1,2,3], Dong Chen[4], Bin Wang[5], Ho-Nam Cheung[1,2,3], Fei Liu[1,2,3], Jianbo Cheng[6], Shankai Tang[7], Zengping Zhang[4], Guolin Feng[3,4,8], and Wenjie Dong[1,2,3]

[1]School of Atmospheric Sciences, Sun Yat-sen University, Zhuhai, China, [2]Key Laboratory of Tropical Atmosphere–Ocean System (Sun Yat-sen University), Ministry of Education, Zhuhai, China, [3]Southern Marine Science and Engineering Guangdong Laboratory, Zhuhai, China, [4]School of Physical Science and Technology, Yangzhou University, Yangzhou, China, [5]Department of Atmospheric Sciences and International Pacific Research Center, University of Hawaii at Manoa, Honolulu, USA, [6]School of Environmental Science and Engineering, Yancheng Institute of Technology, Yancheng, China, [7]School of Atmospheric Sciences, Lanzhou University, Lanzhou, China, [8]National Climate Center, China Meteorological Administration, Laboratory for Climate Studies, Beijing, China

Key Points:

- The long-lasting 2020 Meiyu season was characterized by three stages: advanced-onset, strong-persisting, and delayed withdrawal
- The mid-latitude teleconnection played a crucial role in the 2020 Meiyu onset and withdrawal, while tropical forcing's role is enhanced in the last two stages
- Advanced forecasting systems cannot predict the delayed withdrawal due to the failure in predicting the mid-latitude teleconnection

Supporting Information:

Supporting Information may be found in the online version of this article.

Correspondence to:

G. Feng,
fenggl@cma.gov.cn

Citation:

Qiao, S., Chen, D., Wang, B., Cheung, H.-N., Liu, F., Cheng, J., et al. (2021). The longest 2020 Meiyu season over the past 60 years: Subseasonal perspective and its predictions. *Geophysical Research Letters*, *48*, e2021GL093596. https://doi.org/10.1029/2021GL093596

Received 30 MAR 2021
Accepted 18 APR 2021

Abstract The record-long 2020 Meiyu season since 1961 caused severe floods over the Yangtze and Huaihe River valleys (YHRV). Why the Meiyu duration doubled in 2020 remains a puzzle. We show that the long-lasting Meiyu can be divided into three stages: advanced-onset, strong-persisting, and delayed-withdrawal. The advanced-onset was associated with an extremely negative-phase East Atlantic/West Russia teleconnection. The strong-persisting was attributed to a positive-phase Pacific–Japan (PJ) pattern sustained by La Niña's rapid development. The delayed withdrawal was related to the combined effect of a positive PJ pattern and a mid-troposphere "two ridge–one trough" pattern over Asia. Two subseasonal forecasting systems predicted the positive rainfall anomalies over the YHRV in the first two stages, but not the third stage, which may be associated with poor prediction of the two ridge–one trough pattern. These results highlight the role of subseasonal evolution in extreme climate events.

Plain Language Summary During the northward advance of the East Asian summer monsoon, the East Asian subtropical region is normally characterized by a quasi-stationary rainband that persists from mid-June to mid-July, which is known as Meiyu in China and Baiu in Japan. Both the duration and the accumulated rainfall of the 2020 Meiyu set the highest record since 1961, which caused a severe flood and an enormous economic loss in the Yangtze and Huaihe River valleys (YHRV), central-eastern China. We investigated the mechanism and predictions of this long-lasting flood. The record-long 2020 Meiyu can be divided into three stages: advanced-onset, strong-persisting, and delayed withdrawal. The advanced-onset stage was mainly induced by the extratropical climate anomalies associated with the East Atlantic/West Russia teleconnection. In contrast, the strong-persisting stage was due to the enhanced tropical forcing via triggering the Pacific–Japan pattern. The delayed withdrawal stage arises from the combined effect of tropical forcing and mid-latitude teleconnection. The current advanced forecasting systems can predict the positive rainfall anomalies over the YHRV in the first two stages, but not the third stage. These findings advance our understanding of the extreme 2020 flood and help improve future extreme monsoon prediction.

1. Introduction

Meiyu is a unique rainy season over the Yangtze and Huaihe River valleys (YHRV), which persists from mid-June to mid-July and accounts for about 50% of the accumulated June–July–August (summer) rainfall in the region (Ding & Chan, 2005; Tao & Chen, 1987). The 2020 summer was marked by the longest Meiyu season over the past 60 years, which started on June 1 and ended on August 2 with a duration of 62 days, about twice of the climatology (Ding et al., 2021). The record-long Meiyu season caused accumulated rainfall averaged over the YHRV (28°–33°N, 110°–122°E) exceeding +720 mm (Figure S1a), setting the highest record since 1961 (Figure S1b). The associated severe floods affected about 45.5 million people and caused a direct economic loss of more than 100 billion Chinese Yuan (Wei et al., 2020). An accurate prediction of this kind of extreme event is imperative for agriculture, the economy, and human health.

A central question that needs to be addressed is why 2020 Meiyu lasted so long? One possibility is the abnormal position and intensity of the Western Pacific Subtropical High (WPSH), which are crucial in determining the rainfall anomalies over the YHRV during the Meiyu season (Cui et al., 2020; Ding & Chan, 2005; Song & Zhou, 2014a, b; Wang & Lin, 2002; Ye & Lu, 2011). The 2020 long-lasting Meiyu season was accompanied by the tropical Indian Ocean warming, preceded by a weak central Pacific El Niño event that peaked in 2019/2020 winter and followed by a rapidly developing La Niña event (Figure S2). Y. Takaya et al. (2020) and Zhou et al. (2021) suggested that the tropical Indian Ocean warming was responsible for the extended Meiyu in 2020. However, the western tropical Pacific was even warmer than the northern Indian Ocean (Figure S2), and the abnormal warming over both the northern Indian and western Pacific oceans occurred under the abnormally strong WPSH. The enhanced WPSH can be sustained by remote forcing; it reduces cloudiness and increases downward solar radiation to the ocean surface beneath. Thus, the positive sea surface temperature (SST) anomalies in the northern Indian Ocean and western tropical Pacific likely resulted from enhanced WPSH, rather than a cause of anomalous WPSH (Wang et al., 2004, 2005). Additionally, an enhanced WPSH was found to occur only after a strong El Niño event (Wang et al., 2017), a weak central Pacific El Niño event in 2019/2020 winter was insufficient in sustaining the abnormally strong WPSH in 2020 Meiyu season. On the other hand, the La Niña was rapidly developed from April–May to June–July of 2020 (Figure S2), with the normalized tropical Central Pacific (5°S–5°N/160°E–150°W, the NINO 4 region) SST tendency in May 2020 exceeding −1.42, which is strongly correlated to the accumulated rainfall over the YHRV for the period 1961–2020 ($r = -0.35$, $p < 0.01$; Figure S1b). Because the rapid development of La Niña could be a reason for the enhanced WPSH and Meiyu (Kosaka et al., 2012; Wang et al., 2013; B. Wu et al., 2009), we will elaborate on how the La Niña development contributed to the extreme 2020 Meiyu.

In addition to the tropical SST warming, the extratropical forcing also affects the Meiyu via modulating the WPSH and cold air activities over the subtropical East Asia, including the "two ridge–one trough" pattern over mid-latitude Asia (Ding et al., 2021; Y. Wang, 1992; Q. Zhang & Tao, 1998), the North Atlantic Oscillation (NAO) (Z. Wu et al., 2012), the Silk Road (SR) pattern (Enomoto et al., 2003; Lu et al., 2002; Song et al., 2013) and the circumglobal teleconnection (CGT) pattern (Q. Ding & Wang, 2005; Qiao et al., 2018). Meanwhile, the intraseasonal variability is important to the Meiyu on a subseasonal timescale, which includes the Intraseasonal Oscillation of the East Asian summer monsoon (EASM) (Ding et al., 2020; Lau et al., 1988; B. Wang & Xu, 1997; Zhu et al., 2003), and the Madden-Julian Oscillation (Li et al., 2018; Zhang et al., 2021). As suggested in recent studies, the record-breaking 2020 Meiyu displays a significant characteristic of Quasi-biweekly Oscillation (Ding et al., 2021). The 2020 Meiyu is also regulated by the subseasonal phase transition of the NAO (B. Liu et al., 2020). Different from the emphasis of the role of intraseasonal variability discussed in these studies, we primarily focused on why the 2020 Meiyu lasts so long, which requires examining the roles of extratropical teleconnections on the onset and withdrawal of 2020 Meiyu.

The EASM is characterized by the northward movement of the subtropical frontal zone and associated rain belt from early summer to late summer, with two abrupt jumps associated with the Meiyu season (Y. Ding & Chan, 2005; R. Wu & Wang, 2001). The climate factors affecting the rainfall anomalies differ among early summer, Meiyu season, and late summer (F. Liu et al., 2020). This finding motivates us to examine the subseasonal evolution of the long-lasting 2020 Meiyu. This work specifically addresses two questions regarding the subseasonal variation of the Meiyu rain band in 2020: What are the relative role of extratropical factors and tropical factors in different stages of the evolution? How well do the advanced subseasonal forecasting systems predict these stages? The causes for the success and failure of the predictions are also examined.

We attributed the record-long Meiyu season in 2020 to the advanced-onset and delayed-withdrawal stages during which the mid-latitude teleconnection played a crucial role. La Niña's rapid development played an important role in intensifying rainfall in the strong-persisting and delayed-withdrawal stages. Our understanding gained from this work should help improve seasonal and subseasonal predictions of East Asian extreme floods.

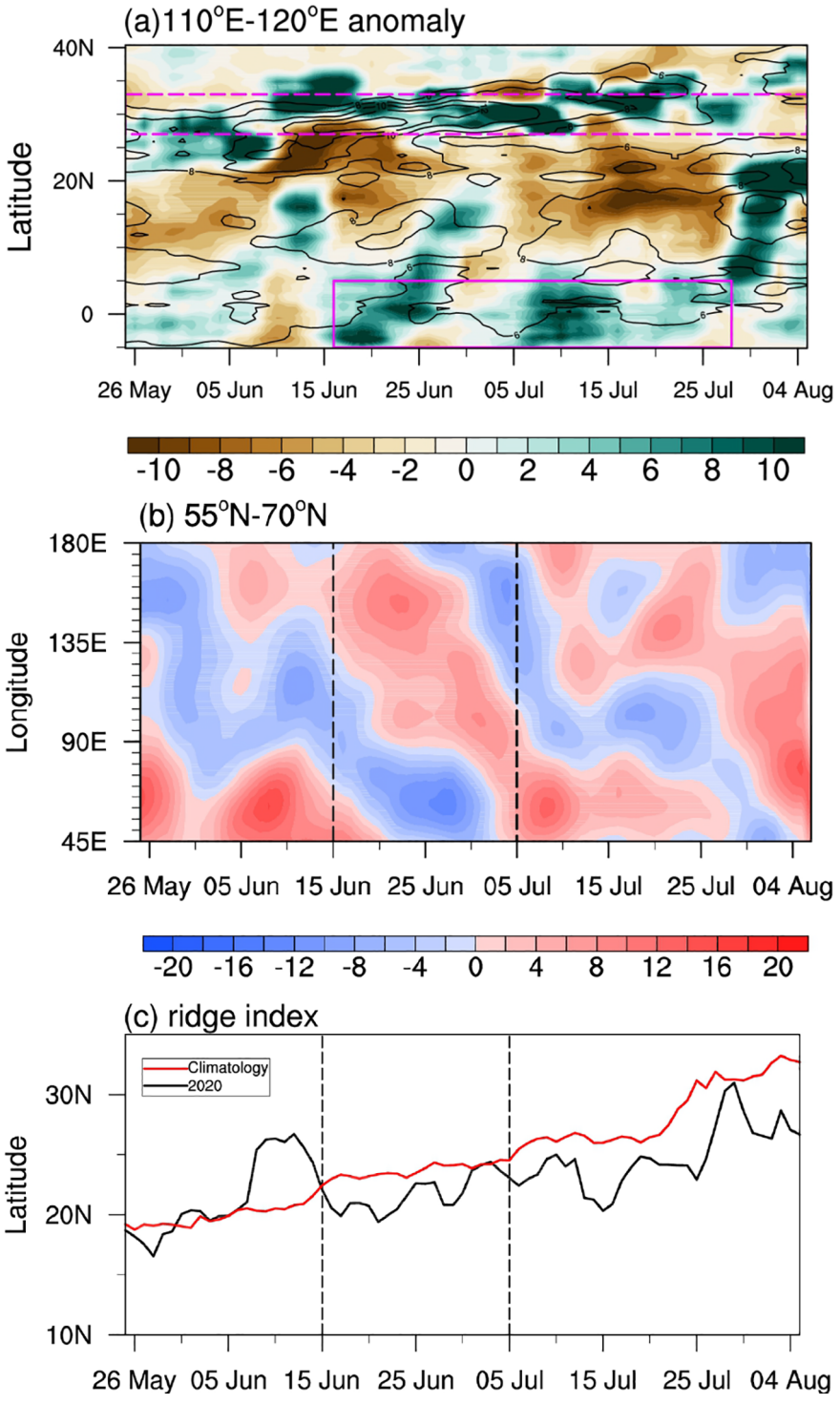

Figure 1. (a) Time-latitude cross section of the 5-days running-mean rainfall in climatology (contour interval: 2 mm day^{-1}) and rainfall anomalies in the year 2020 (shading; mm day^{-1}) averaged over 110°–120°E from May 25 to August 5. (b) Time-latitude cross-section of 5-days running mean 500-hPa stream function anomalies (shading; 10^6 m^2 s^{-1}) averaged over 55°–70°N from May 25 to August 5. (c) Evolution of the ridge line of the WPSH in climatology (red line) and year 2020 (black line) from May 25 to August 5. The climatology is based on the period 1982–2019. The daily rainfall data and atmospheric variables are from the ERA5. ERA5, European Center for Medium Range Weather Forecasts Reanalysis 5; WPSH, western Pacific subtropical high.

2. Data and Methods

The hourly rainfall, 500-hPa geopotential height, zonal and meridional components of wind at 850 hPa, and surface air temperature (SAT) from 1979 to 2020 were extracted from the European Center for Medium Range Weather Forecasts Reanalysis 5 (ERA5), with a horizontal resolution of 0.25° × 0.25°. The hourly data were converted to daily data before analysis. The daily SST data from 1982 to 2020 were taken from the Optimum Interpolation Sea Surface Temperature, version 2 (OISSTv2), and has a resolution of 0.25° × 0.25° (Reynolds et al., 2002). Additionally, the monthly SST data provided by the Extended Reconstructed SST version 5 (ERSST5) (from 1854 to 2020; Huang et al., 2017), and the daily rainfall of 2,479 in situ observations provided by the National Meteorological Information Center in China (from 1951 to 2020) was used. The daily and monthly anomalies of these variables are the departures from the 38-years climatology (1982–2019). To exclude the possible influence of regional warming on the results (L. Liu et al., 2021), all data have been detrended prior to analysis. The statistical significance tests are conducted by the two-tailed Student's t-test using the effective number of degrees of freedom (J. Li et al., 2013; Pyper & Peterman, 1998).

The model forecast data include the daily fields of the European Center for Medium Range Weather Forecasts (ECMWF) and National Centers for Environmental Prediction (NCEP) from the subseasonal to seasonal (S2S) Prediction Project Database (Vitart et al., 2017) because both models well predicted the rainfall anomalies in East Asia within one week in advance (Jie et al., 2017; S. Li & Robertson, 2015). In this study, the forecast data initialized at 0000 UTC on 25 May, 8 June, and 29 June were selected to assess the prediction skills of the three stages. These initial dates lead the beginnings of each stage by about one week. The anomalies of the forecast data in each stage were calculated with respect to the model's climatology. The ensemble-mean forecast is the unweighted average of 51 (16) members for the ECMWF (NCEP) model, with a forecast range extending up to 46 (44) days.

The stationary wave activity flux (Takaya & Nakamura 1997, 2001) is employed to depict Rossby wave propagation. The Pacific–Japan (PJ) pattern and SR pattern are defined as the first empirical orthogonal function mode of the summer-mean 850-hPa relative vorticity over 0°–60°N/100°–140°E (Kosaka & Nakamura, 2010) and the summer-mean 200-hPa meridional wind anomalies over 20°–60°N/60°–150°E (Yasui & Watanabe, 2010), respectively. The CGT pattern is defined by 200-hPa height anomalies averaged over 35°–40°N/60°–70°E (Q. Ding & Wang, 2005). The observed or predicted daily climate indices (e.g., East Atlantic/West Russia (EA/WR) pattern index, the NAO index, the PJ pattern index, and the SR pattern index) are acquired by projecting the daily anomalies onto the associated observed regression pattern of the summer-mean indices. The ridgeline latitude of the WPSH is defined as the averaged latitudinal position where the 850-hPa zonal wind to be zero in the 500-hPa 5870-gpm contour domain between 110°E and 150°E, similar to that in Y. Liu et al. (2014).

3. Results

3.1. Three-Stage Evolution of 2020 Meiyu Season

Although the extended Meiyu season in 2020 persisted from June 1 to August 2 (Ding et al., 2021), we focus on the positive rainfall anomalies over the YHRV before 28 July, because the positive rainfall anomalies moved to the north of 33°N after July 28 (Figure 1a). The rain band shifted northward before mid-June, enhanced in late June and early July, and shifted southward after mid-July (Figure 1a), when considering the location of the strongest rainfall anomalies relative to its climatological location. The accompanied transitions occurred in the wave train anomalies across mid-latitude Asia (45°–120°E) around mid-June and early July, where positive stream function anomalies were located at the Urals in the first and third stages, and near Lake Baikal (~100°E) in the second stage (Figure 1b). The selection of latitude band 55°–70°N is due to frequent blocking anticyclones there. Compared to the climatology, the WPSH is located more northward (southward) before (after) June 15 (Figure 1c), and the positive rainfall anomalies over the Maritime Continent abruptly enhanced on June 15 and July 5 (Figure 1a), respectively. These results suggest different Meiyu evolutions among the three stages. Accordingly, the entire period is divided into three stages: advanced-onset stage (June 1–15), strong-persisting stage (June 16– July 5), and delayed-withdrawal stage (July 6–28). Note that the following results are not sensitive to slight changes of the starting or ending times for each stage.

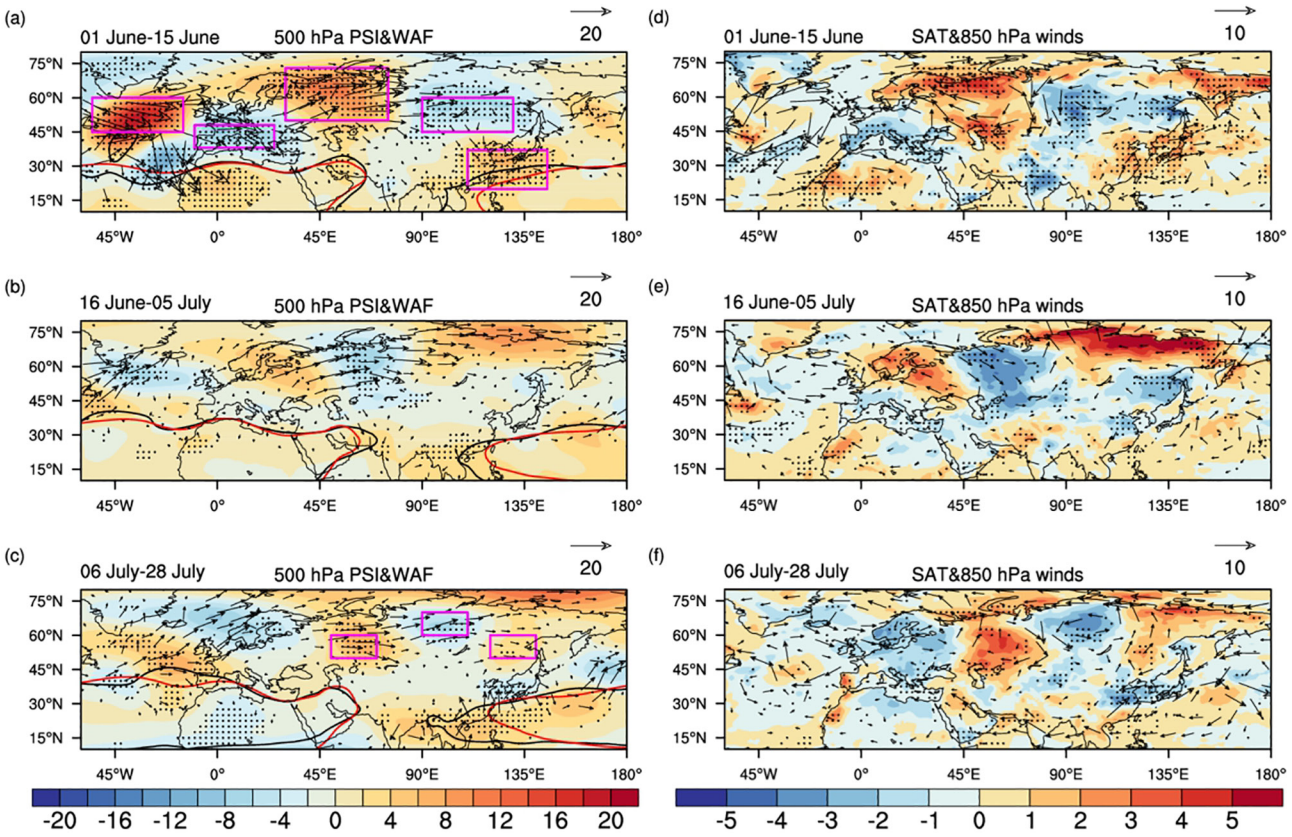

Figure 2. Maps of 500-hPa stream function anomalies (shading; 10^6 m^2 s^{-1}) and associated horizontal wave activity flux (vector; m^2 s^{-2}) averaged (a) between 1 June and 15 June, (b) between 16 June and 5 July, and (c) between July 6 and July 28 in 2020. (d), (e) and (f) are the same as (a), (b) and (c), respectively, but for showing SAT anomalies (shading; °C) and 850-hPa wind anomalies (vector; m s^{-1}). *Note.* that in (a)–(c) the black (red) contour represents the 5,870-gpm isopleth of the 500-hPa geopotential height in climatology (year 2020). Stippling in (a)–(c) and (d)–(f) represents 500-hPa stream function anomalies and SAT anomalies exceeding one standard deviation, respectively. The five magenta rectangles in (a) denote the basic location of the five centers of action for the EA/WR pattern. The three magenta rectangles in (c) denote the basic location of the three centers of action for the ridge–one trough pattern. The atmospheric variables are from the ERA5. ERA5, European Center for Medium Range Weather Forecasts Reanalysis 5; EA/WR, East Atlantic/West Russia; SAT, surface air temperature.

3.2. Different Roles of Tropical and Extratropical Factors in Each Stage

To identify the extratropical and tropical factors associated with the Meiyu rain bands during the three stages, 500-hPa stream function anomalies and their associated horizontal wave activity flux are shown in Figures 2a–c, while the associated 850-hPa wind anomalies and SAT anomalies are shown in Figures 2d–f. In the advanced-onset stage, the stream function anomalies over the North Atlantic and mid-latitude Eurasia were characterized by two negative centers of action over Europe and Lake Baikal, and three positive centers over the central North Atlantic, the Urals, and subtropical East Asia (Figure 2a). These strongly resembled the negative phase of the EA/WR pattern (Barnston & Livezey, 1987), with the most negative EA/WR index (−2.46) during the study period (Figure 3a). The pattern correlation coefficient (PCC) between the stream function anomalies in 2020 and the EA/WR regression pattern over 30°–70°N/60°W–180°E is −0.73, which is much higher in magnitude than the PCCs with the regression patterns of NAO (+0.39), SR (−0.25) and CGT (−0.03) (Figure S3). The result suggests the stronger impact of the extremely negative EA/WR pattern than other patterns in this stage. Moreover, the associated positive stream function anomalies over subtropical East Asia (25°–40°N) accompanied a northwestward expansion of the WPSH (Figure 2a) and an anticyclonic anomaly over the subtropical western north Pacific (Figure 2d), which shifted the rainband northward (Figure 1a) and produced above-normal rainfall (+4.46 mm day^{-1}) over the YRHV, particularly in its northern part (Figure S4a). The ridgeline of the WPSH is significantly correlated to the EA/WR index ($r = -0.35$, $p < 0.05$) in June 1–15 for the period 1981–2020. The above results suggest a crucial role of the EA/WR pattern in the advanced-onset of 2020 Meiyu.

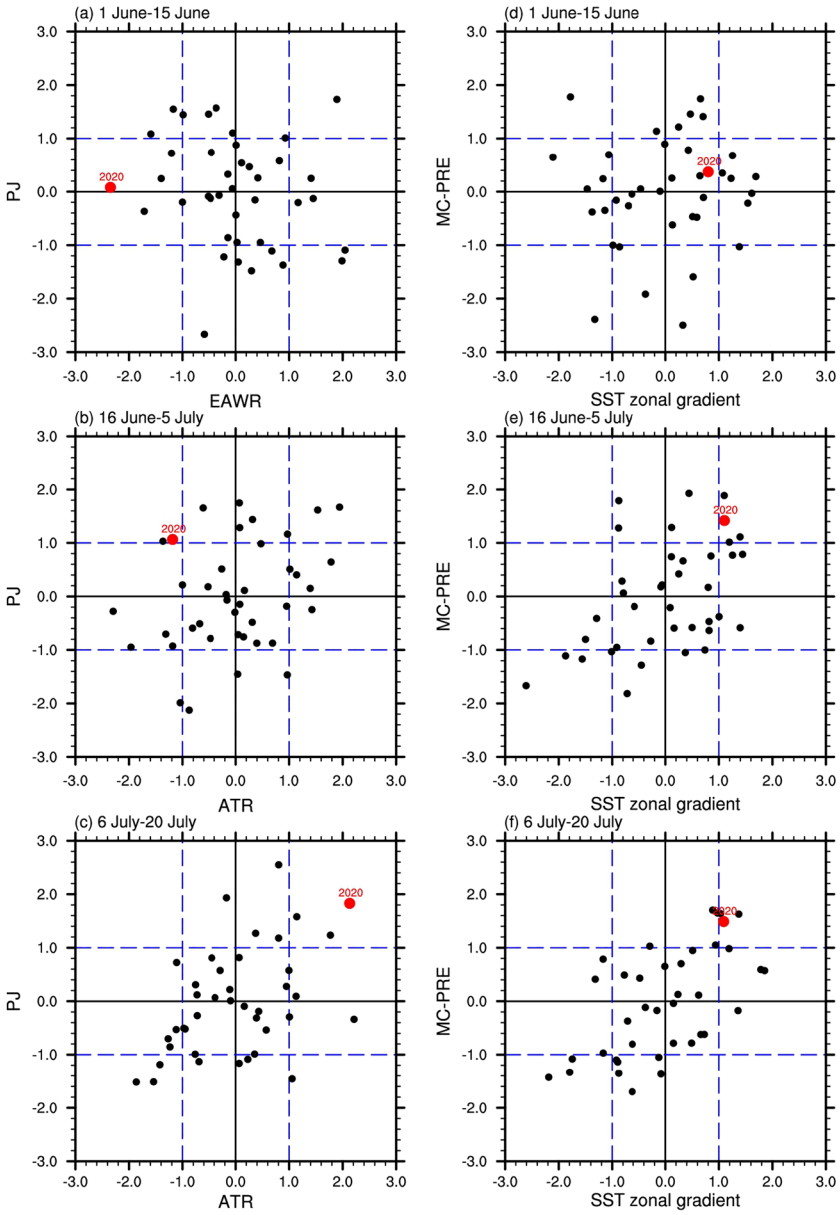

Figure 3. Scatterplot of normalized time series of (a) the EA/WR index and PJ index averaged between June 1 and June 15, and the ATR index and PJ index averaged (b) between June 16 and July 5, and (c) between July 6 and July 28 for the period 1981–2020. (d), (e) and (f) are the same as (a), (b) and (c), respectively, but for the scatterplot of normalized time series of SST gradient between the 5°S–5°N/120°–150°E and the 5°S–5°N/170°E–160°W (see the magenta rectangles in Figures 4a–c) and rainfall anomalies averaged over the Maritime Continent (5°S–5°N/100°–130°E) (see the magenta rectangles in Figures 4d–f) for the period 1982–2020. The dotted lines indicate one standard deviation, and the red dots represent the anomalies in the year 2020. The rainfall and atmospheric indices were calculated from the ERA5. The SST zonal gradient index was calculated from the OISSTv2. ATR, Asian trough ridge; ERA5, European Center for Medium Range Weather Forecasts Reanalysis 5; EAWR, East Atlantic West Russia; PJ, Pacific Japan; SST, sea surface temperature.

In the strong-persisting stage, the 500-hPa stream function anomalies over mid-latitude Eurasia were almost opposite to those in the advanced-onset stage, but the propagation of the Rossby wave train shifted to a higher latitude than in the first stage (Figures 2a–b). Accordingly, mid-latitude Asia aloft was characterized by two troughs over the Urals and the Okhotsk Sea and one ridge over northern Lake Baikal (Figure 2b). On the other hand, the positive stream function anomalies over the western tropical North Pacific (10°–25°N) persisted during the two stages. In addition to slightly negative stream function anomalies over

the mid-latitude western North Pacific (30°–45°N), a positive PJ pattern (Kosaka & Nakamura, 2010; Nitta, 1987; Xu et al., 2018) was established, and wave activity flux propagated northwards along the East Asian coast (Figure 2b). These anomalous circulations were associated with a southwestward expansion of the WPSH (Figure 2b) and stronger cold air activity over subtropical East Asia (Figure 2e), which produced a much larger rainfall anomaly (+5.52 mm day^{-1}) over the YHRV (Figure S4b).

In the delayed-withdrawal stage, the positive PJ pattern persisted and strengthened. This accompanied stronger wave activity flux emanating from the tropical Pacific to mid-latitude East Asia (Figure 2b vs. Figure 2c). The persistence of the positive PJ pattern was accompanied persistently by the southwestward expansion of the WPSH (Figure 2c), and the strengthening of the PJ pattern transported more water vapor towards the YHRV via the WPSH. On the other hand, the stream function anomalies over mid-latitude Eurasia were reversed to those in the second stage, and the trough–ridge pattern over mid-latitude Asia changed to two ridges over the Urals and northeastern China, respectively, and one trough over northern Lake Baikal (Figures 2b–c), which were favorable for cold air activity over subtropical East Asia (Figure 2f) and prevented the climatological northward jump of the WPSH. Altogether, the positive rainfall anomalies (+7.39 mm day^{-1}) over the YHRV reached the peak in this stage (Figure S4c).

Clearly, the relative roles of the extratropical factors and tropical factors differed in the three stages. The advanced-onset stage was mainly associated with an extremely negative phase of the EA/WR pattern (Figure 3a). The strong-persisting stage was associated with a positive PJ index (+1.07) (Figure 3b), which may be induced by record-breaking warm SST over the western North Atlantic in May 2020 (Zheng & Wang, 2021). The persistently positive PJ index (+1.83) and positive Asian trough–ridge (ATR) index (+2.43) jointly contributed to the delayed-withdrawal stage(Figure 3c). Here, the ATR index is used to represent the two ridge–one trough pattern, which is defined as the difference of 500-hPa stream function anomalies between those averaged over 50°–60°N/50°–70°E and 50°–60°N/120°–140°E and those averaged over 60°–70°N/90°–110°E (see the magenta rectangles in Figure 2c) (Q. Zhang & Tao 1998). It is noteworthy that the rainfall anomalies over the YHRV associated with the key climate indices during the three stages for the period 1981–2020 were basically consistent with the 2020 Meiyu case, particularly for the first two stages (Figure S4 vs. Figure S5). The slight inconsistency in the last stage might be associated with the linear regression's limitation in representing the joint effects of the two factors. The above results suggest a crucial role of extratropical factors in the onset and withdrawal of 2020 Meiyu, while the tropical factor's role enhanced in the last two stages.

Previous studies have shown that the developing La Niña increases the SST zonal gradients in the western equatorial Pacific and enhances the rainfall in the Maritime Continent, both of which play an important role in triggering a positive PJ pattern and an enhanced WPSH (Kosaka et al., 2012; Wang et al., 2013). To investigate the possible roles of the developing La Niña in the latter two stages, we compare the anomalies of SST, rainfall, and 850-hPa winds in the three stages. Apparently, the resultant SST zonal gradient in the western equatorial Pacific strengthened from the advanced-onset stage to the subsequent two stages (Figures 4a–c), as evidenced by the SST gradient between 5°S–5°N/120°–150°E and 5°S–5°N/170°E−160°W (see the magenta rectangles in Figures 4a–c) exceeding one standard deviation in the latter two stages, but it was weakest in the first stage (Figures 3d–f). Note that the result was not sensitive to the slight changes of the longitudinal extent used in defining the SST zonal gradient in the equatorial western Pacific. Meanwhile, the easterly wind anomalies and enhanced rainfall in the Maritime Continent were evident in the latter two stages but not the first stage (Figures 4d–f). Thus, the La Niña development played an important role in the southwestward expansion of the WPSH and the associated long-lasting rainfall over the YHRV in the latter two stages.

3.3. Real-Time Subseasonal Prediction

To assess the predictability of the three-stage Meiyu season in 2020, we compare the observed and predicted rainfall anomalies in each stage. Both models reproduced the positive rainfall anomalies over the YRHV in the first two stages. The NCEP (ECMWF) model performed better in the advanced-onset (strong-persisting) stage, when the predicted rainfall anomalies over the YRHV exceeding +0.99 (+0.93) mm day^{-1} (Figures S4e, g). Both models predicted the negative EA/WR pattern in the advanced-onset stage (Figure 5a; Figures s6a, d). Although the two peaks of observed positive PJ index were not reproduced by both models

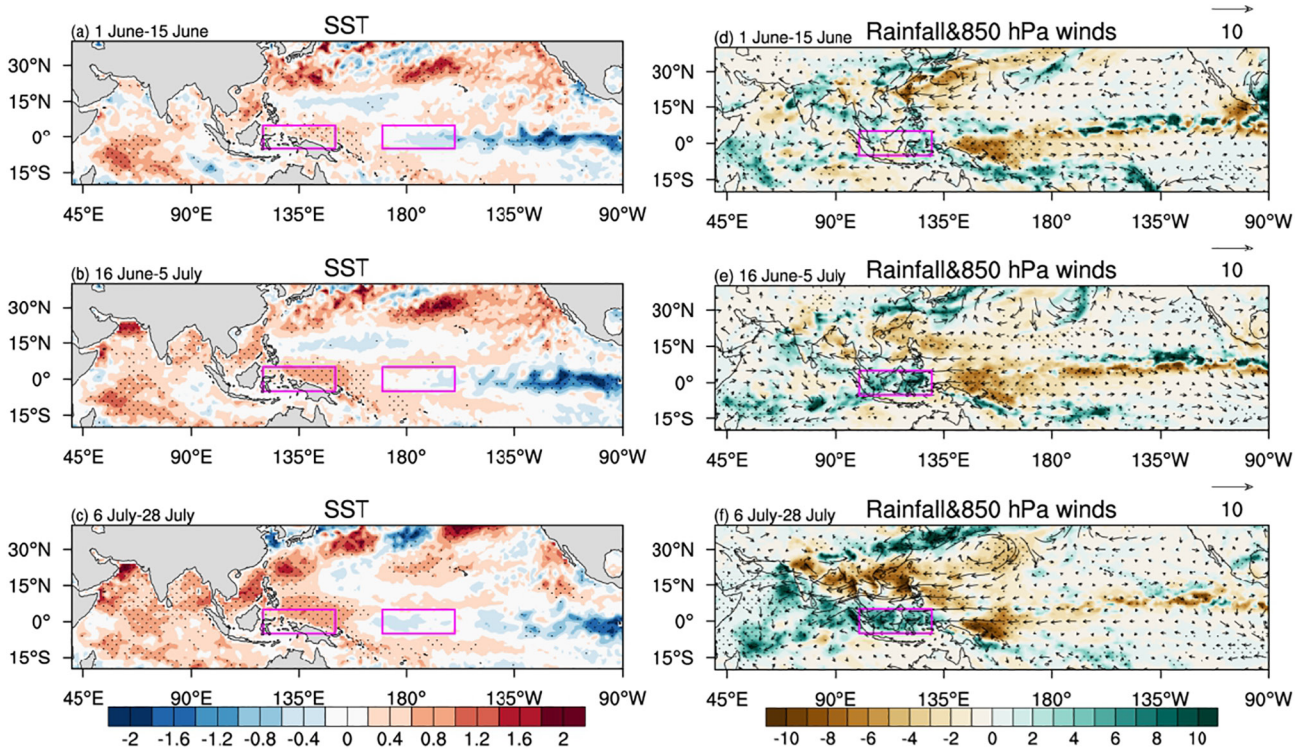

Figure 4. Observed SST anomalies (shading; °C) averaged (a) between June 1 and June 15, (b) between June 16 and July 5, and (c) between July and July 28 in the year 2020. (d), (e) and (f) are the same as (a), (b) and (c), respectively, but for rainfall anomalies (shading; mm day^{-1}) and 850-hPa wind anomalies (vector; m s^{-1}). Stippling in (a)–(c) and (d)–(f) represents SST anomalies and rainfall anomalies exceeding one standard deviation, respectively. The two magenta rectangles in (a)–(c) denote the two regions that are used to define the SST zonal gradient in the equatorial western Pacific. The magenta rectangle in (d)–(f) denotes the region that used to define rainfall anomalies over the Maritime Continent. The daily SST data are from the OISSTv2, and the daily rainfall and 850-hPa winds are from the ERA5. ERA5, European Center for Medium Range Weather Forecasts Reanalysis 5; SST, sea surface temperature.

in the strong-persisting stage, the predicted PJ index averaged in this stage (+0.74 for ECMWF; +0.62 for NCEP) coincided well with that of the observed PJ index (+0.75) (Figure 5b). In contrast, the excessive rainfall over the YRHV in the delayed-withdrawal stage was not predicted by both models, with the NCEP model even predicting a negative rainfall anomaly of −1.96 mm day^{-1} (Figures S4f and i). Despite both models predicted a positive PJ index (Figure 5c), the predicted two centers of action of the positive PJ pattern were shifted northward compared to the observations (Figure 3c vs. Figure S6c; Figure 3c vs. Figure S6f), which corresponded to a northward shift of the rain band and a large bias of the rainfall anomalies over the YRHV (Figures S4f, i). The poor prediction of the PJ pattern location in the delayed-withdrawal stage may be associated with the poor prediction of the two ridge−one trough pattern (Figure 5d), which is further evidenced by the fact that the ridge over northeastern China could not be predicted by both models (Figures S6c, f); this failure led to less cold air activities over subtropical East Asia and promoted a northward shift of the PJ pattern.

4. Conclusions and Discussion

The record-high 2020 Meiyu rainfall since 1961 (Figure S1) could be divided into three stages: advanced-onset stage, strong-persisting stage, and delayed-withdrawal stage. As shown in Figure S7, the advanced-onset stage featured the northwestward expansion of the WPSH associated with an extremely negative EA/WR teleconnection pattern. The strong-persisting stage was associated with a positive PJ pattern and the accompanying southwestward expansion of the WPSH. The persistently positive PJ pattern and two ridge−one trough patterns over mid-latitude Asia jointly contributed to the delayed-withdrawal stage. The persistence of the positive PJ pattern during the latter two stages was primarily associated with the La Niña development. The subseasonal forecasting systems of the ECMWF and NCEP predicted the positive sign of rainfall

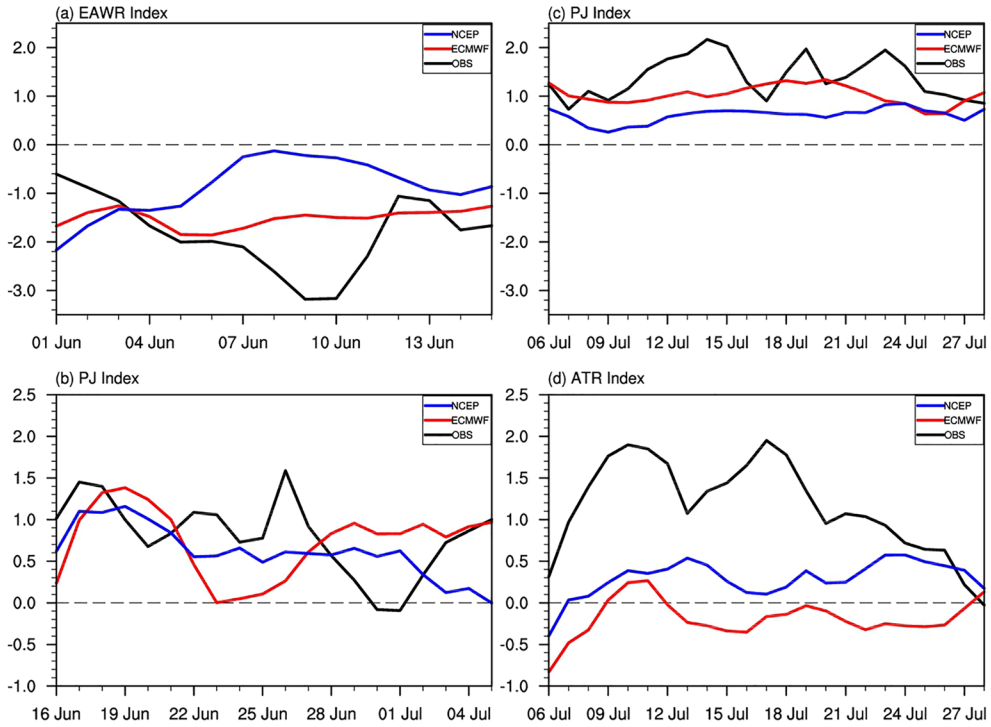

Figure 5. Observed (black line) and predicted (red line for the ECMWF model, blue for the NCEP model) EA/WR index from June 1 to June 15 of 2020. (b), (c), and (d) are the same as (a), but for the PJ index from June 16 to July 5, the PJ index from July 6 to July 28, and the ATR index from July 6 to July 28, respectively. *Note* that the predictions were initialized on May 25 for (a), on June 8 for (b), and on June 29 for (c) and (d). The observed atmospheric indices are calculated from the ERA5. ATR, Asian trough ridge; ERA5, European Center for Medium Range Weather Forecasts Reanalysis 5; EA/WR, East Atlantic/West Russia; ECMWF, European Center for Medium Range Weather Forecasts; NCEP, National Centers for Environmental Prediction; PJ, Pacific Japan.

anomalies and the associated large-scale circulation features in the first two stages, including the negative EA/WR pattern in the advanced-onset stage and the positive PJ pattern in the strong-persisting stage.

Consider that the mid-latitude circulation anomalies in the delayed-withdrawal stage can be better represented by the "two ridge–one trough" pattern than other known teleconnection patterns (Figure S8), the relationship between the two ridge–one trough pattern and the well-known teleconnection patterns over Eurasia deserves further studies. Meanwhile, apart from the effect of La Niña development highlighted during the latter two stages in this study, some studies suggested that the tropical Indian Ocean warming (Figure S2e) may contribute to the extended 2020 Meiyu via the coupled Indo-western Pacific Ocean capacitor (Ding et al., 2021; Takaya et al., 2020; Zhou et al., 2021). As discussed in the introduction, the relative role of the warm Indian Ocean and the La Niña development is an open question, calling for further clarification by numerical experiments. Compared to isolated tropical (Takaya et al., 2020; Zhang et al., 2021; Zhou et al., 2021) or extratropical (B. Liu et al., 2020) factors in the 2020 extreme long-lasting Meiyu, our results demonstrate the role of a combination of both and highlight the three-stage evolution forming this extreme monsoon event. The new seasonal prediction system should benefit from considering the subseasonal variability. The poor prediction of the third stage in both state-of-the-art forecasting systems calls for urgent improvement of simulating mid-latitude variability.

Data Availability Statement

The ERA5 data were available at https://cds.climate.copernicus.eu/cdsapp#!/search?text=ERA5&type=-dataset. The OISSTv2 data were downloaded from https://www.esrl.noaa.gov/psd/data/gridded/data.noaa.oisst.v2.html. The ERSST5 data were taken from https://psl.noaa.gov/data/gridded/data.noaa.ersst.v5.html. The subseasonal to seasonal (S2S) Prediction Project Database were retrieved from https://apps.ecmwf.int/

datasets/data/s2s-realtime-instantaneous-accum-ecmf/levtype=sfc/type=cf/. The monthly mean EA/WR, NAO, and Niño four indices were available at the NOAA Climate Prediction Center (CPC) website https://www.cpc.ncep.noaa.gov/data/teledoc/eawruss.shtml.

Acknowledgements
The authors acknowledge the support of the National Key Research and Development Program of China (2017YFC1502300), the Key Program of the National Natural Science Foundation of China (41530531), the General Program of the National Natural Science Foundation of China (41905057, 41905050, 41975088, and 41875100), and the China Postdoctoral Science Foundation funded project (2018M640848).

References

Barnston, A. G., & Livezey, R. E. (1987). Classification, seasonality, and persistence of low-frequency atmospheric circulation patterns. *Monthly Weather Review*, *115*, 1083–1126. https://doi.org/10.1175/1520-0493(1987)115<1083:CSAPOL>2.0.CO;2

Cui, W., Dong, X., Xi, B., & Liu, M. (2020). Cloud and precipitation properties of MCSs along the Meiyu frontal zone in central and southern China and their associated large-scale environments. *Journal of Geophysical Research: Atmospheres*, *125*(6), e2019JD031601. https://doi.org/10.1029/2019JD031601

Ding, Q., & Wang, B. (2005). Circumglobal teleconnection in the Northern Hemisphere summer. *Journal of Climate*, *18*(17), 3483–3505. https://doi.org/10.1175/JCLI3473.1

Ding, Y., & Chan, J. C. L. (2005). The East Asian summer monsoon: An overview. *Meteorology and Atmospheric Physics*, *89*(1), 117–142. https://doi.org/10.1007/s00703-005-0125-z

Ding, Y., Liang, P., Liu, Y., & Zhang, Y. (2020). Multiscale variability of Meiyu and its prediction: A new review. *Journal of Geophysical Research: Atmospheres*, *125*(7), e2019JD031496. https://doi.org/10.1029/2019JD031496

Ding, Y., Liu, Y., & Hu, Z. (2021). The Record-breaking Meiyu in 2020 and associated atmospheric circulation and tropical SST anomalies. *Advances in Atmospheric Sciences*. https://doi.org/10.1007/s00376-021-0361-2

Enomoto, T., Hoskins, B. J., & Matsuda, Y. (2003). The formation mechanism of the Bonin high in August. *Quarterly Journal of the Royal Meteorological Society*, *129*(587), 157–178. https://doi.org/10.1256/qj.01.211

Huang, B., Thorne, P. W., Banzon, V. F., Boyer, T., Chepurin, G., Lawrimore, J. H., et. al. (2017). Extended reconstructed sea surface temperature, version *5* (ERSSTv5): Upgrades, validations, and intercomparisons. *Journal of Climate*, *30*(20), 8179–8205. https://doi.org/10.1175/JCLI-D-16-0836.1

Jie, W., Vitart, F., Wu, T., & Liu, X. (2017). Simulations of the Asian summer monsoon in the sub-seasonal to seasonal prediction project (S2S) database. *Quarterly Journal of the Royal Meteorological Society*, *143*(706), 2282–2295. https://doi.org/10.1002/qj.3085

Kosaka, Y., Chowdary, J. S., Xie, S. P., Min, Y. M., & Lee, J. L. (2012). Limitations of seasonal predictability for summer climate over East Asia and the Northwestern Pacific. *Journal of Climate*, *25*(21), 7574–7589. https://doi.org/10.1175/JCLI-D-12-00009.1

Kosaka, Y., & Nakamura, H. (2010). Mechanisms of meridional teleconnection observed between a summer monsoon system and a subtropical anticyclone. Part I: The pacific–japan pattern. *Journal of Climate*, *23*(19), 5085–5108. https://doi.org/10.1175/2010JCLI3413.1

Lau, K. M., Yang, G. J., & Shen, S. H. (1988). Seasonal and intraseasonal climatology of summer monsoon rainfall over Eeat Asia. *Monthly Weather Review*, *116*(1), 18–37. https://doi.org/10.1175/1520-0493(1988)116<0018:SAICOS>2.0.CO;2

Li, J., Sun, C., & Jin, F. F. (2013). NAO implicated as a predictor of Northern Hemisphere mean temperature multidecadal variability. *Geophysical Research Letters*, *40*(20), 5497–5502. https://doi.org/10.1002/2013GL057877

Li, S., & Robertson, A. W. (2015). Evaluation of sub-monthly precipitation forecast skill from global ensemble prediction systems. *Monthly Weather Review*, *143*(7), 2871–2889. https://doi.org/10.1175/MWR-D-14-00277.1

Liu, B., Yan, Y., Zhu, C., Ma, S., & Li, J. (2020). Record-breaking Meiyu rainfall around the Yangtze River in 2020 regulated by the subseasonal phase transition of the North Atlantic Oscillation. *Geophysical Research Letters*, *47*(22), e2020GL090342. https://doi.org/10.1029/2020GL090342

Liu, F., Ouyang, Y., Wang, B., Yang, J., Ling, J., & Hsu, P. C. (2020). Seasonal evolution of the intraseasonal variability of China summer precipitation. *Climate Dynamics*, *54*(11–12), 4641–4655. https://doi.org/10.1007/s00382-020-05251-0

Liu, L., Wang, X., Feng, G., Dogar, M. M., Zhang, F., Zhiqiang, G., & Zhou, B. (2021). Variation of main rainy-season precipitation in eastern China and relevance to regional warming. *International Journal of Climatology*. *41*(3), 1767–1783. https://doi.org/10.1002/joc.6929

Liu, Y., Li, W., Zuo, J., & Hu, Z. (2014). Simulation and projection of the western Pacific subtropical high in CMIP5 models. *Journal of Meteorological Research*, *28*(3), 327–340. https://doi.org/10.1007/s13351-014-3151-2

Li, X., Gollan, G., Greatbatch, R. J., & Lu, R. (2018). Intraseasonal variation of the East Asian summer monsoon associated with the Madden–Julian oscillation. *Atmospheric Science Letters*, *19*(4), e794. https://doi.org/10.1002/asl.794

Lu, R. Y., Oh, J. H., & Kim, B. J. (2002). A teleconnection pattern in upper-level meridional wind over the North African and Eurasian continent in summer. *Tellus*, *54*(1), 44–55. https://doi.org/10.3402/tellusa.v54i1.12122

Nitta, T. (1987). Convective activities in the tropical western Pacific and their impact on the Northern Hemisphere summer circulation. *Journal of the Meteorological Society of Japan*, *65*(3), 373–390. https://doi.org/10.2151/jmsj1965.65.3_373

Pyper, B. J., & Peterman, R. M. (1998). Comparison of methods to account for autocorrelation in correlation analyses of fish data. *Canadian Journal of Fisheries and Aquatic Sciences*, *55*(9), 2127–2140. https://doi.org/10.1139/f98-104

Qiao, S., Hu, P., Feng, T., Cheng, J., Han, Z., Gong, Z., et al. (2018). Enhancement of the relationship between the winter Arctic Oscillation and the following summer circulation anomalies over central East Asia since the early 1990s. *Climate Dynamics*, *50*(9–10), 3485–3503. https://doi.org/10.1007/s00382-017-3818-3

Reynolds, R. W., Rayner, N. A., Smith, T. M., Stokes, D. C., & Wang, W. (2002). An improved in situ and satellite SST analysis for climate. *Journal of Climate*, *15*(13), 1609–1625. https://doi.org/10.1175/1520-0442(2002)015<1609:aiisas>2.0.co;2

Song, F., & Zhou, T. (2014a). Interannual variability of East Asian summer monsoon simulated by CMIP3 and CMIP5 AGCMs: Skill dependence on Indian Ocean–Western Pacific anticyclone teleconnection. *Journal of Climate*, *27*(4), 1679–1697. https://doi.org/10.1175/JCLI-D-13-00248.1

Song, F., & Zhou, T. (2014b). The climatology and inter-annual variability of East Asian summer monsoon in CMIP5 coupled models: Does air-sea coupling improve the simulations? *Journal of Climate*, *27*(23), 8761–8777. https://doi.org/10.1175/JCLI-D-14-00396.1

Song, F., Zhou, T., & Wang, L. (2013). Two modes of the Silk Road pattern and their interannual variability simulated by LASG/IAP AGCM SAMIL2.0. *Advances in Atmospheric Sciences*, *30*(3), 908–921.Retrieved from https://link.springer.com/article/10.1007/s00376-012-2145-1

Takaya, K., & Nakamura, H. (1997). A formulation of a wave-activity flux for stationary Rossby waves on a zonally varying basic flow. *Geophysical Research Letters*, *24*(23), 2985–2988. https://doi.org/10.1029/97GL03094

Takaya, K., & Nakamura, H. (2001). A formulation of a phase-independent wave activity flux for stationary and migratory quasigeostrophic eddies on a zonally varying basic flow. *Journal of the Atmospheric Sciences*, *58*(6), 608–627. https://doi.org/10.1175/1520-0469(2001)058<0608:afoapi>2.0.co;2

Takaya, Y., Ishikawa, I., Kobayashi, C., Endo, H., & Ose, T. (2020). Enhanced Meiyu-Baiu rainfall in early summer 2020: Aftermath of the 2019 super IOD event. *Geophysical Research Letters*, *47*(22), e2020GL090671. https://doi.org/10.1029/2020GL090671

Tao, S., & Chen, L. (1987). In C. P. Chang, & T. N. Krishnamurti (Eds.), Eds., *A review of recent research on the East Asian summer monsoon in China*. Monsoon Meteorology (pp. 60–92). Oxford University Press. Retrieved from https://ci.nii.ac.jp/naid/10012388648

Vitart, F., Ardilouze, C., Bonet, A., Brookshaw, A., Chen, M., Codorean, C., et al. (2017). The subseasonal to seasonal (S2S) prediction project database. *Bulletin of the American Meteorological Society*, *98*(1), 163–173. https://doi.org/10.1175/BAMS-D-16-0017.1

Wang, B., Ding, Q., Fu, X., Kang, I. S., Jin, K., Shukla, J., & Doblas-Reyes, F. (2005). Fundamental challenge in simulation and prediction of summer monsoon rainfall. *Geophysical Research Letters*, *32*(15), L15711. https://doi.org/10.1029/2005GL022734

Wang, B., Kang, I. S., & Lee, J. Y. (2004). Ensemble simulations of Asian-Australian monsoon variability by 11 AGCMs. *Journal of Climate*, *17*(4), 803–818. https://doi.org/10.1175/1520-0442(2004)017<0803:esoamv>2.0.co;2

Wang, B., Li, J., & He, Q. (2017). Variable and robust East Asian monsoon rainfall response to El Niño over the past 60 years (1957-2016). *Advance in Atmospheric Sciences*, *34*(10), 1235–1248. https://doi.org/10.1007/s00376-017-7016-3

Wang, B., & Lin, H. (2002). Rainy season of the Asian-Pacific summer monsoon. *Journal of Climate*, *15*(4), 386–398. https://doi.org/10.1175/1520-0442(2002)015<0386:rsotap>2.0.co;2

Wang, B., Xiang, B. Q., & Lee, J. Y. (2013). Subtropical high predictability establishes a promising way for monsoon and tropical storm predictions. *Proceedings of the National Academy of Sciences of the United States of America*, *110*(8), 2718–2722. https://doi.org/10.1073/pnas.1214626110

Wang, B., & Xu, X. (1997). Northern hemisphere summer monsoon singularities and climatological intraseasonal oscillation. *Journal of Climate*, *10*(5), 1071–1085. https://doi.org/10.1175/1520-0442(1997)010<1071:nhsmsa>2.0.co;2

Wang, Y. (1992). Effects of blocking anticyclones in Eurasia in the rainy season (Meiyu/Baiu season). *Journal of the Meteorological Society of Japan*, *70*(5), 929–951. https://doi.org/10.2151/jmsj1965.70.5_929

Wei, K., Ouyang, C., Duan, H., Li, Y., & Zhou, S. (2020). Reflections on the catastrophic 2020 Yangtze River Basin flooding in southern China. *The Innovation*, *1*(2), 100038. https://doi.org/10.1016/j.xinn.2020.100038

Wu, B., Zhou, T., & Li, T. (2009). Seasonally evolving dominant interannual variability modes of East Asian climate. *Journal of Climate*, *22*(11), 2992–3005. https://doi.org/10.1175/2008JCLI2710.1

Wu, R., & Wang, B. (2001). Multi-stage onset of the summer monsoon over the western north pacific. *Climate Dynamics*, *17*(4), 277–289. https://doi.org/10.1007/s003820000118

Wu, Z., Li, J., Jiang, Z., He, J., & Zhu, X. (2012). Possible effects of the North Atlantic Oscillation on the strengthening relationship between the East Asian Summer monsoon and ENSO. *International Journal of Climatology*, *32*(5), 794–800. https://doi.org/10.1002/joc.2309

Xu, P., Wang, L., Chen, W., Feng, J., & Liu, Y. (2018). Structural changes in the Pacific–Japan pattern in the late 1990s. *Journal of Climate*, *32*(2), 607–621. https://doi.org/10.1175/JCLI-D-18-0123.1

Yasui, S., & Watanabe, M. (2010). Forcing processes of the summertime circumglobal teleconnection pattern in a dry AGCM. *Journal of Climate*, *23*(8), 2093–2114. https://doi.org/10.1175/2009JCLI3323.1

Ye, H., & Lu, R. Y. (2011). Subseasonal variation in ENSO-related East Asian rainfall anomalies during summer and its role in weakening the relationship between the ENSO and summer rainfall in Eastern China since the late 1970s. *Journal of Climate*, *24*(9), 2271–2284. https://doi.org/10.1175/2010JCLI3747.1

Zhang, Q., & Tao, S. (1998). Influence of Asian mid–high latitude circulation on East Asian summer rainfall (in Chinese). *Acta Meteorologica Sinica*, *56*(2), 199–211. https://doi.org/10.11676/qxxb1998.019

Zhang, W., Huang, Z., Jiang, F., Stuecker, M. F., Chen, G., & Jin, F. (2021). Exceptionally persistent Madden-Julian Oscillation activity contributes to the extreme 2020 East Asian summer monsoon rainfall. *Geophysical Research Letters*, *48*, e2020GL091588. https://doi.org/10.1029/2020GL091588

Zheng, J., & Wang, C. (2021). Influences of three oceans on record-breaking rainfall over the Yangtze River Valley in June 2020. *Science China Earth Sciences*, *64*. https://doi.org/10.1007/s11430-020-9758-9

Zhou, Z., Xie, S. P., & Zhang, R. (2021). Historic Yangtze flooding of 2020 tied to extreme Indian Ocean conditions. *Proceedings of the National Academy of Sciences of the United States of America*, *118*(12), e2022255118. https://doi.org/10.1073/pnas.2022255118

Zhu, C., Nakazawa, T., Li, J., & Chen, L. (2003). The 30–60 day intraseasonal oscillation over the western North Pacific Ocean and its impacts on summer flooding in China during 1998. *Geophysical Research Letters*, *30*(18), 1952. https://doi.org/10.1029/2003GL017817